Recibido 27 Septiembre 2018, aceptado 4 Diciembre 2018, fecha de publicación 16 Diciembre 2018

ISSN 2448-7775

Microgrids Primary Controls: A Review

GIBRAN AGUNDIS-TINAJERO[1], JUAN SEGUNDO-RAMÍREZ[1], NANCY VISARO-CRUZ[1]

[1]Centro de Investigación y Estudios de Posgrado, Facultad de Ingeniería, Universidad Autónoma de San Luis Potosí, San Luis Potosí, México.
gibran.zigma@gmail.com
j2ramirez@gmail.com
nvisairoc@uaslp.mx

ABSTRACT This paper presents a review of basic primary controls for the operation of grid-connected and islanded AC microgrids, furthermore, synchronization schemes for power converters are addressed. Detailed information about the control structures and their block diagrams are presented; additionally, several examples are included to show the performance of the controls, their advantages and drawbacks.

KEYWORDS Current-control schemes, voltage-control schemes, islanded microgrid, phase-locked-loop.

I. INTRODUCTION

For more than one century, centralized electric power generation has been used to feed the industrial and domestic electric demand across the world; however, in the last decades, the research and development of renewable energy technologies have been increasing and getting stronger, such that, the use of distributed generation (DG) units with power electronic interface (DC/AC or AC/DC/AC) is becoming more common in electric power systems such as AC and DC microgrids (MG) [1]-[3]. A microgrid is commonly defined as a small-scale system, formed by DG units, energy storage systems (ESS), and loads, which are interconnected and work properly in a controlled manner. Additionally, a MG should be able to operate in grid-connected or islanded mode [4]. In the grid-connected mode, the MG share active and reactive power with the main grid in case of a power deficit or an excess of generated power, furthermore, the microgrid can provide ancillary services and it would be seen by the main system as a single controlled element. In the islanded mode, power generated within the microgrid, have to be in balance with the demand of local loads, with regulated frequency and bus voltages.

Since the microgrid concept was developed, a big research effort has been focused to maximize the reliability and potential benefits that the microgrids can offer. Some of the issues that can be found on microgrids, arise from assumptions commonly applied to conventional power systems which are invalid for MGs [3], [4]. In this way, in the past years, many new control schemes were proposed to cope with different issues that can be found in MGs, such as, voltage droops, frequency deviations, power quality, power sharing, among others. On the other hand, in the microgrid environment, characterized by having frequent changes in topology, changes in demand-supply balance, interactions between controllers, and bidirectional power flow, robustness and adaptiveness of controllers were desired features [3], [4]. Nontheless, most of the control improvements have been based on basic primary control schemes for both, grid-connected and islanded mode.

Regarding the aforementioned, in this paper a review of basic primary controls for the operation of grid-connected and islanded AC microgrids is carried out. Firstly, synchronization schemes for electric power converters are addressed, then, three different control schemes, including current-controlled and voltage-controlled strategies are shown.

II. PRIMARY CONTROLS FOR AC MICROGRIDS

The primary controls are the first level in the control hierarchy, featuring the fastest response. Primary controls are used to share power with the main grid or to feed a local load in a controlled manner by means of local measurements; this can be done via controlling the current injected by the DG unit or controlling the voltage of the inverter output. Resulting in current and voltage controlled strategies [3]-[6].

The current-controlled strategies are used to inject active and reactive power, lacking the capacity to regulate the system frequency or voltage, so they need to work connected to the grid or together with another DG which regulates the frequency and voltage of the MG. In this way, the regulation of the system frequency and voltage can be achieved using voltage-controlled inverters [4]. In any case, the DG units need to be synchronized with the system if it is connected to the main grid, such that they

can work properly. For each different control scheme, the needed information can be the phase angle, the frequency, and the voltage amplitude.

A. SYNCHRONIZATION OF POWER CONVERTERS

The synchronization task is often defined as the procedure of matching a source with an existing power system so that they are able to work in parallel. During this process, the phase angle, voltage, and frequency of the DG unit are synchronized with the power system [7]. On the other hand, the information provided by the synchronization unit, in addition to the initial synchronization task, are also very useful for different monitoring/control purposes, such as the reference current generation for the converter, adapting controllers to the grid frequency variations, islanding detection, among others [8], [9].

1. Phase-Locked Loop

A phase-locked loop (PLL) is a nonlinear control system which synchronizes its output in frequency and phase with its input. Three basic parts can be found in almost all PLLs [8], [9]:

- Phase detector (PD): This unit provides a signal which contains the phase error information, i.e., the difference between the real and estimated phase angle.
- Loop filter (LF): The LF is mainly responsible to filter the AC components of the PD output. The PLL tracking characteristics are also mainly dictated by the LF.
- Voltage-controlled oscillator (VCO): This part generates a sinusoidal signal in its output, with the same phase angle as the integral of the LF output.

Within three-phase systems, the synchronous reference frame PLL (SRF-PLL) is a standard, being the basic block of almost all advanced PLLs (see Fig. 1) [9].

From this block diagram, the small signal model can be derived for tuning procedure and stability analysis. The block diagram of the small-signal model is shown in Fig. 2.

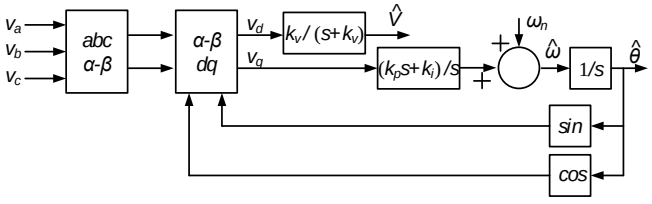

Fig. 1. SRF-PLL block diagram.

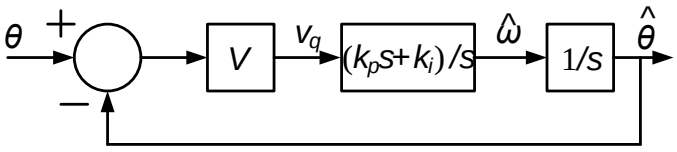

Fig. 2. SRF-PLL small-signal block diagram.

The selection of the gains can be computed using the SRF-PLL characteristic polynomial from the closed-loop transfer function,

$$G_{cl}(s)=V(k_p s+k_i)/(s^2+Vk_p s+Vk_i) \quad (1)$$

where V is the voltage magnitude of the system, and k_p, k_i are the proportional and integral gains, respectively.

Using the standard design approach available for second-order systems, the proportional and integral gains are defined as $Vk_i=\omega_n^2$ and $Vk_p=2\xi\omega_v$, where the damping factor is denoted by ξ and the natural frequency by ω. The damping factor mainly determines the stability margin and the dynamic response damping, and the natural frequency mainly dictates the speed of transient response of the SRF-PLL.

On the other hand, to analyze and understand some behaviors of the SRF-PLL, the open-loop transfer function is obtained,

$$G_{ol}(s)=V(k_p s+k_i)/s^2 \quad (2)$$

Note from (2) that the voltage amplitude is proportional to the loop gain. Thus, the grid voltage amplitude variations change the loop gain, affecting the dynamic behavior of the SRF-PLL. To deal with this problem, the voltage amplitude normalization is included in the SRF-PLL scheme as can be seen in Fig. 3 and a performance comparison is shown in Fig. 4.

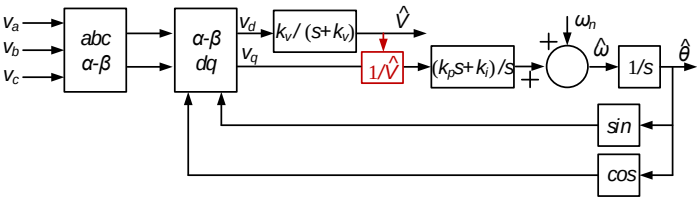

Fig. 3. SRF-PLL block diagram with normalization.

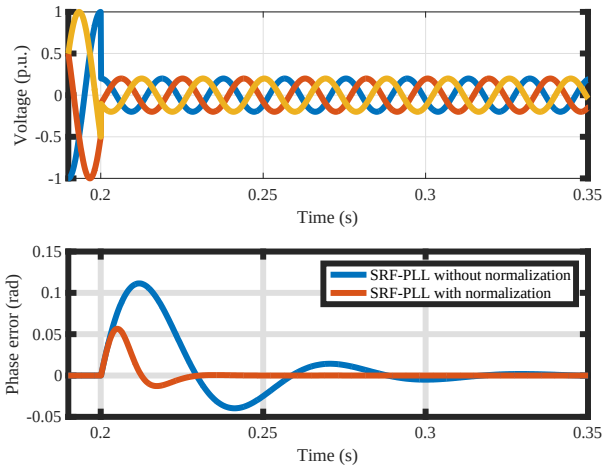

Fig. 4. SRF-PLL performance with and without amplitude normalization, in response to a voltage sag with 3 Hz frequency jump.

2448-7775©2018 Identidad Energética

On the other hand, from (2) it can be seen that the control system has two open-loop poles at the origin. Therefore, the SRF-PLL scheme fails in achieving a zero steady-state error for frequency ramps. If a zero steady-state phase error in response to frequency ramps is desired, another open-loop poles should be created using an integrator [10] as can be seen in the Fig. 5, additionally, in Fig. 6 the performance with and without the extra integrator is shown.

Recently, in [10] an enhanced implementation of SRF-PLL was presented. This enhanced SRF-PLL prevents a large overshoot transients in the estimated frequency during phase jumps and grid faults, and provides a higher filtering capability in the estimation of the grid frequency. The enhanced SRF-PLL scheme is shown in Fig. 7 and a comparison of its performance against the conventional one is shown in Fig. 8.

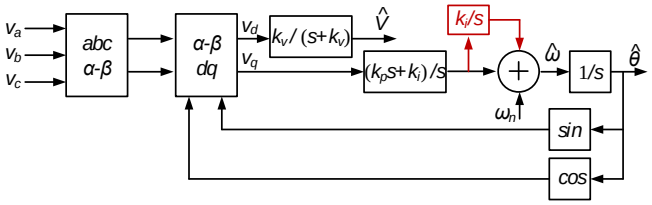

Fig. 5. SRF-PLL block diagram with an extra integrator.

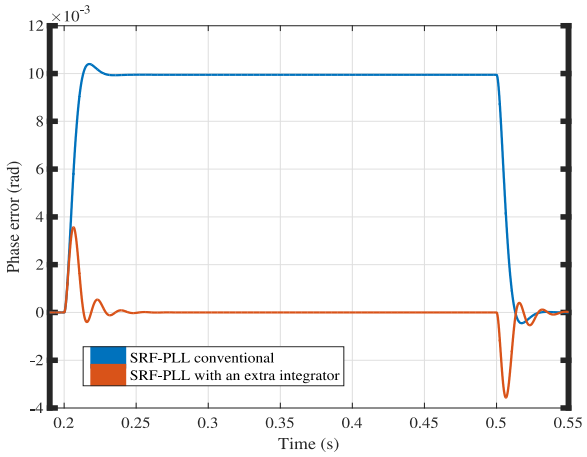

Fig. 6. SRF-PLL performance with and without the extra integrator, in response to a 30 Hz frequency ramp.

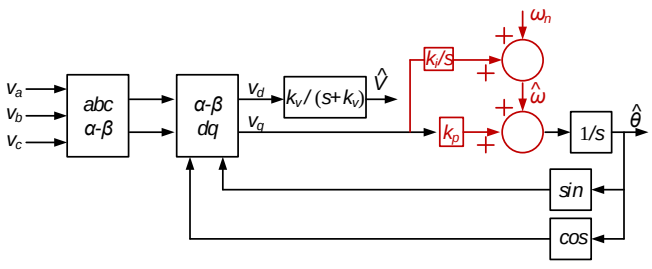

Fig. 7. Enhanced SRF-PLL block diagram.

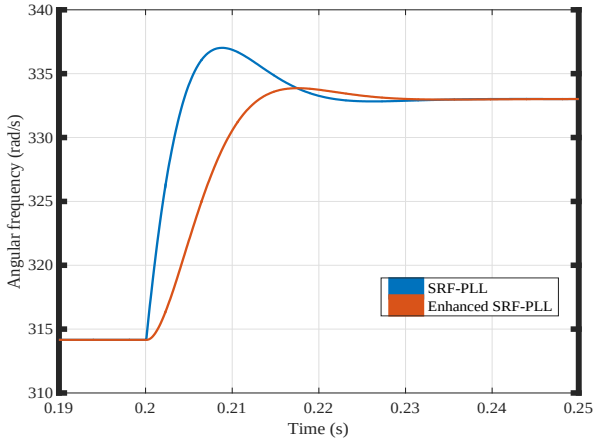

Fig. 8. Performance comparison between the conventional SRF-PLL and the Enhanced SRF-PLL in response to a 3 Hz frequency jump.

Worth mentioning that, the conventional SRF-PLL is a very effective synchronization tool when the grid voltage is balanced and without harmonic distortion. In the presence of DC offset, harmonics, and imbalance in the grid voltage the performance of SRF-PLL is significantly degraded. In this way, in recent years advanced three-phase PLL have been proposed. These PLLs are often implemented by including different filters in the SRF-PLL control scheme [11]-[13].

B. GRID-FORMING DROOP-BASED CONTROL

The grid-forming power converters are controlled working as AC voltage sources having as references the amplitude V^* and frequency ω^* [14]. Under islanded operation, the voltage magnitude and frequency of the system have to be regulated, therefore, at least one DG unit assumes this task [14], [15]. In this scheme, the power injection of each DG unit of the islanded system is defined by the frequency/active power (P-ω) and voltage/reactive power (Q-V) droop characteristics [16],

$$\omega = \omega^* - K_n^P P_n \quad (3)$$

$$V_n = V^* - K_n^q Q_n \quad (4)$$

where, ω^* is the angular frequency, V_n^* is the voltage amplitude, and K_n^P and K_n^q are the droop coefficients [16]. As shown in Fig. 9, the droop characteristics define the angular frequency of the MG, and the voltage of each DG unit; thus, the percentage of active and reactive power injected by each DG.

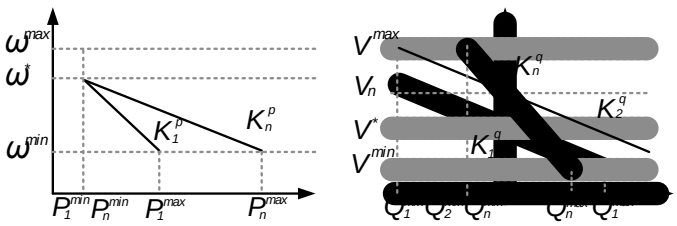

Fig. 9. Conventional droop characteristics [13].

The control scheme, which is shown in Fig. 10, is composed of droop control loops, a voltage control loop, a current control loop, and stages for signal transformation from *abc* to *dq* and vice versa [14].

A small example is presented below to show the behavior of the primary control. The test case (see Fig. 11) includes two controlled DG units connected through LCL filters to a point of common coupling (PCC), additionally, a resistive load is connected to the PCC as well. The parameters of the current and voltage control loops are shown in Table I.

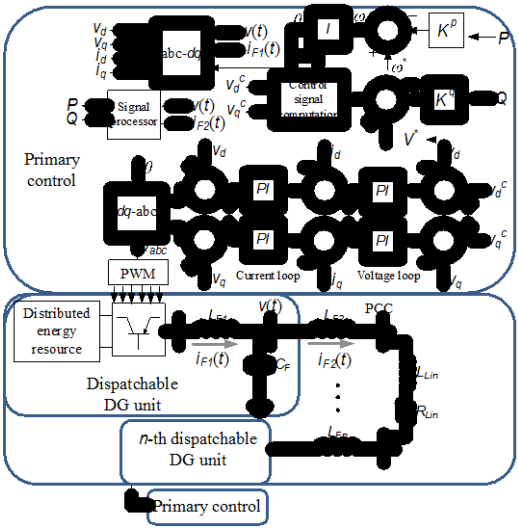

Fig. 10. **Basic grid-forming control structure [11].**

TABLE I. **PARAMETERS FOR THE ISLANDED MICROGRID CONTROL.**

Parameter	Symbol	Value
Current loop proportional gain	k_{pc}	20
Current loop integral gain	k_{ic}	40
Voltage loop proportional gain	k_{pv}	2.4e-2
Voltage loop integral gain	k_{iv}	4.5

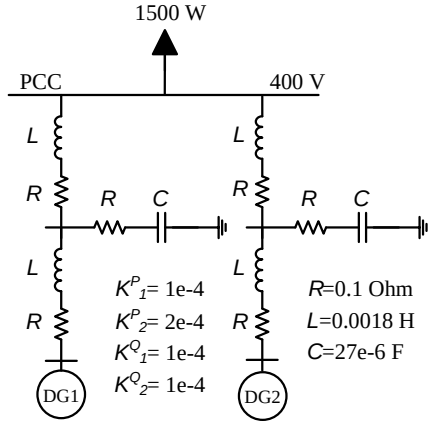

Fig. 11. **Single line diagram of the three-phase test system.**

The system is energized and the load is connected at $t = 0.5$ s. In Fig. 12 the PCC voltage and the injected active power of each DG unit is shown. Observe that, due to the droop coefficients, the DG 2 injects the half of the power injected by DG 1. On the other hand, the controlled DG units could achieve a stable steady-state starting from zero and maintain stable after the load connection.

C. GRID-FEEDING CONTROL

Grid-feeding power converters are controlled as current sources; these power converters can be operated in parallel with other power converters. The references for this control are the active and reactive power, therefore, they are not able to operate in island mode if the voltage and frequency of the system are not adjusted, for example with a grid-forming power converter, or a local synchronous generator.

Fig. 13 shows a basic grid-feeding structure, it includes a PLL to synchronize with the system and a current control loop. The active and reactive power references of the control, are often set by a high level controller, such as an optimal power sharing. Note that in this controller, the *dq* current references I_{dref} and I_{qref}, are computed using the information of the power references and the *dq* voltage in the connection point as shown below,

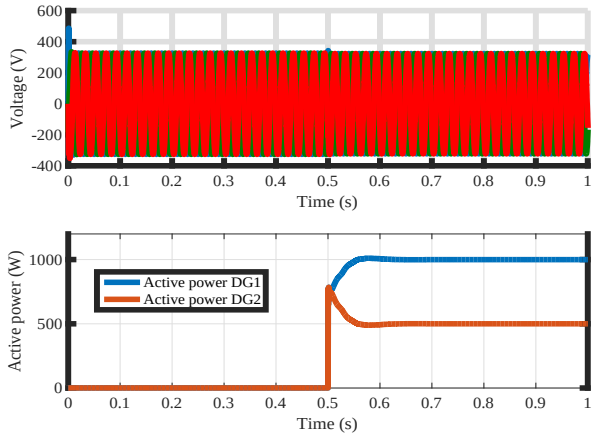

Fig. 12. **PCC voltage and DG units injected active power during an energization and load connection.**

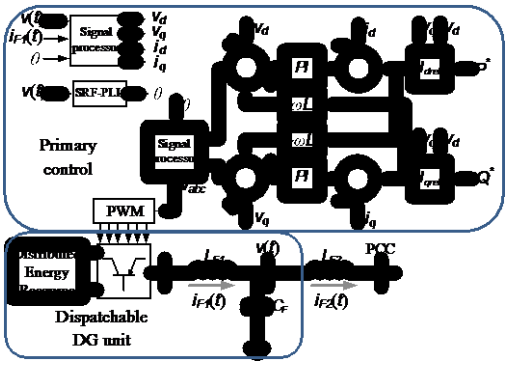

Fig. 13. **PCC voltage and DG units injected active power during an energization and load connection.**

$$I_{dref}=(P^*v_d+Q^*v_q)/((3/2)(v_d^2+v_q^2)) \quad (5)$$
$$I_{qref}=(P^*v_d-Q^*v_q)/((3/2)(v_d^2+v_q^2)) \quad (6)$$

where P^* and Q^* are the active and reactive power references, respectively, and v_d and v_q are the dq voltage measured in the capacitor.

A test case is presented below to show the grid-feeding control behavior. In Fig. 14 the single line diagram of the three-phase system is shown, it includes two DG units which are connected to PCC and it is connected to the main grid. In this case, the system is connected to the main grid and after 6 cycles the DG units start working with active power references of 500 W and 300 W, DG1 and DG2, respectively. The proportional and the integral gains used in the control, are the same used in the islanded MG example.

It can be seen in Fig. 15 the results in terms of the active power injected by each DG unit. Note that after the connection of the DG units, the power sharing achieves the steady-state in 0.18 seconds, following the active power references.

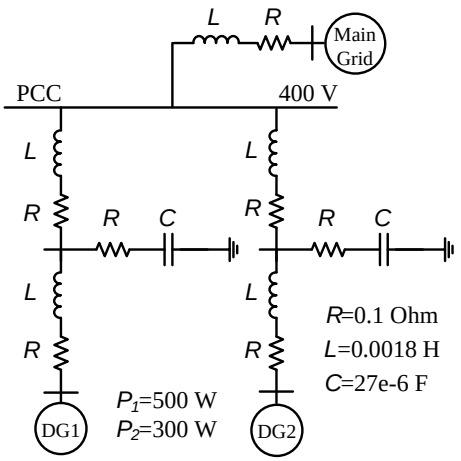

Fig. 14. **Single line diagram of the three-phase test system for the connected case.**

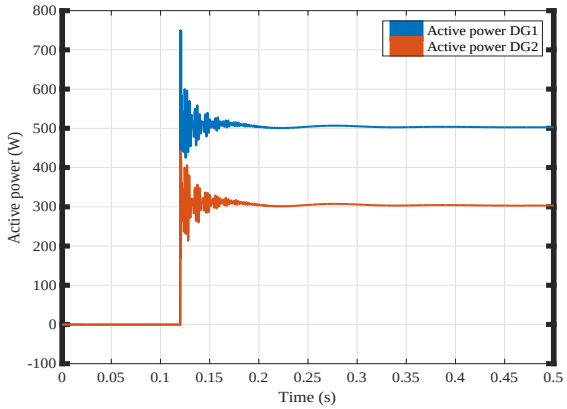

Fig. 15. **Injected active power by the DG units.**

D. PROPORTIONAL-RESONANT CONTROL

The proportional-resonant (PR) controller is a control that can be used for both, grid connected or islanded mode. This control scheme includes a proportional and a resonant term [17], [18],

$$C_{PR}(s)=k_p+k_i s/(s^2+\omega^2) \quad (7)$$

where ω is the resonant frequency, k_p the proportional gain and k_i the resonant gain. This control has a high gain around the resonant frequency such that the steady-state error when tracking or rejecting a sinusoidal signal is zero. Furthermore, in order to improve the performance, a harmonic compensator can be included and is given by [18],

$$C_{PRH}(s)=\Sigma_{h=1,2,3\ldots} k_{ih}s/(s^2+(\omega h)^2) \quad (8)$$

where h is the harmonic order and k_{ih} the harmonic resonant gain.

It is worth noting that, the disadvantage of this scheme is that if the frequency of the system varies, the performance of the controller is degraded. In this way, if the system frequency varies significantly, adaptive mechanisms should be adopted.

A PR controller is usually used in the stationary reference (α-β) frame for inverter control, therefore, only two voltages need to be controlled with two separate PR controllers. The block diagram of a voltage-controlled converter with the PR controller is shown in Fig. 16.

If the controller is used as a current-controller, a PLL is needed to generate the information to synchronize with the system. In the case of a voltage-controller the voltage reference could be made using a droop control as shown in subsection *B*. Finally, the outputs of the PR controllers are converted into PWM (Pulse Width Modulation) signals to drive the switches [18].

To shown the performance of the PR control, a case study is evaluated. The case study has the same electrical structure as Fig. 16, it includes a controlled DG unit, a LCL filter and a load connected to the PCC. The system parameters are shown in Table II.

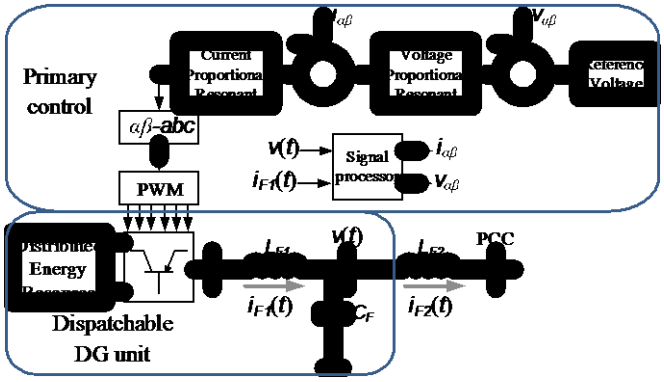

Fig. 16. **Basic proportional-resonant control structure.**

TABLE II. **PARAMETERS FOR THE PR CONTROL.**

Parameter	Symbol	Value
Current loop proportional gain	k_{pc}	10
Current loop integral gain	k_{ic}	200
Voltage loop proportional gain	k_{pv}	1e-2
Voltage loop integral gain	k_{iv}	50
Fifth harmonic gain	k_{i5}	50
Seventh harmonic gain	k_{i7}	50
Eleventh harmonic gain	k_{i11}	250

The system is energized and the steady-state PCC voltage signals including a resistive load, a nonlinear load (diode bridge) and a nonlinear load but using harmonic rejection are shown in Figures 17(a), 17(b), and 17(c), respectively.

Note that, including only the resistive load, the voltage signals in the PCC do not have any harmonic distortion; however, when the nonlinear load is connected the signal get distorted with a THD of 3.51%. On the other side, including the harmonic rejection control for the 5th, 7th and 11th harmonics, it can be seen in Fig. 17(c) that the harmonic content is reduced with a THD of 1.50%.

III. CONCLUSIONS

A review of basic primary controls, such as, grid-feeding, grid-forming and proportional-resonant, were addressed. Different synchronization techniques (PLLs) and the PR harmonic rejection were included. Additionally, detailed information about the control structures were given in each subsection.

Several examples of the reviewed controls were performed in order to show their performance. Furthermore, the results obtained shown the advantages and drawbacks of each control in the different microgrid modes, i.e., grid-connected and islanded mode.

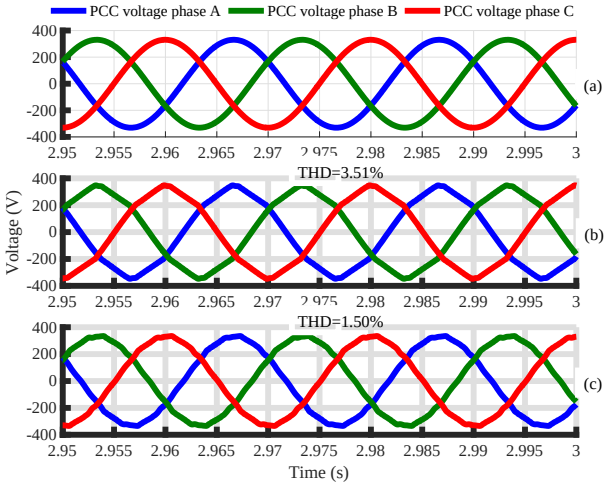

Fig. 17. **Basic proportional-resonant control performance.**

REFERENCES

[1] R. Lasseter, "Microgrids," in IEEE Power Engineering Society Winter Meeting, 2002., vol. 1, 2002, pp. 305–308, vol.1.

[2] N. Hatziargyriou, H. Asano, R. Iravani, and C. Marnay, "Microgrids," Power and Energy Magazine, IEEE, vol. 5, no. 4, pp. 78–94, July 2007.

[3] S. Chowdhury and P. Crossley, Microgrids and Active Distribution Networks, ser. IET renewable energy series. Institution of Engineering and Technology, 2009.

[4] D. E. Olivares, A. Mehrizi-Sani, A. H. Etemadi, C. A. Cañizares, R. Iravani, M. Kazerani, A. H. Hajimiragha, O. Gomis-Bellmunt, M. Saeedifard, R. Palma-Behnke, G. A. Jiménez-Estévez, and N. D. Hatziargyriou, "Trends in microgrid control," IEEE Transactions on Smart Grid , vol. 5, no. 4, pp. 1905–1919, July 2014.

[5] T. L. Vandoorn, J. C. Vasquez, J. D. Kooning, J. M. Guerrero, and L. Vandevelde, "Microgrids: Hierarchical control and an overview of the control and reserve management strategies," IEEE Industrial Electronics Magazine, vol. 7, no. 4, pp. 42–55, Dec 2013.

[6] J. M. Guerrero, J. C. Vsquez, and R. Teodorescu, "Hierarchical control of droop-controlled dc and ac microgrids: a general approach towards standardization," in 2009 35th Annual Conference of IEEE Industrial Electronics, Nov 2009, pp. 4305–4310.

[7] R. C. Schaefer, "Art of generator synchronizing," IEEE Transactions on Industry Applications , vol. 53, no. 1, pp. 751–757, Jan 2017.

[8] F. Gardner, Phaselock Techniques. Wiley, 2005.

[9] S. Golestan, J. M. Guerrero, and J. C. Vasquez, "Threephase plls: A review of recent advances," IEEE Transactions on Power Electronics, vol. 32, no. 3, pp. 1894–1907, March 2017.

[10] S. Golestan, M. Monfared, F. D. Freijedo, and J. M. Guerrero, "Advantages and challenges of a type-3 pll," IEEE Transactions on Power Electronics , vol. 28, no. 11, pp. 4985–4997, Nov 2013.

[11] X. Guo, W. Wu, and Z. Chen, "Multiple-complex coefficient-filter-based phase-locked loop and synchronization technique for three-phase grid-interfaced converters in distributed utility networks," IEEE Transactions on Industrial Electronics, vol. 58, no. 4, pp. 1194–1204, April 2011.

[12] Y. F. Wang and Y. W. Li, "Analysis and digital implementation of cascaded delayed-signal-cancellation pll," IEEE Transactions on Power Electronics , vol. 26, no. 4, pp. 1067–1080, April 2011.

[13] Y. F. Wang and Y. W. Li, "Grid synchronization pll based on cascaded delayed signal cancellation," IEEE Transactions on Power Electronics , vol. 26, no. 7, pp. 1987–1997, July 2011.

[14] J. Rocabert, A. Luna, F. Blaabjerg, and P. Rodr´ıguez, "Control of power converters in ac microgrids," IEEE Transactions on Power Electronics , vol. 27, no. 11, pp. 4734–4749, Nov 2012.

[15] J. A. P. Lopes, C. L. Moreira, and A. G. Madureira, "Defining control strategies for microgrids islanded operation," IEEE Transactions on Power Systems , vol. 21, no. 2, pp. 916–924, May 2006.

[16] J. Guerrero, L. Garcia De Vicuna, J. Matas, M. Castilla, and J. Miret, "A wireless controller to enhance dynamic performance of parallel inverters in distributed generation systems," IEEE Transactions on Power Electronics , vol. 19, no. 5, pp. 1205–1213, Sept 2004.

[17] Q.C. Zhong and T. Hornik. "Control of Power Inverters in Renewable Energy and Smart Grid Integration". Wiley - IEEE. Wiley, 2012. ISBN 9781118481790.

[18] F. Blaabjerg, R. Teodorescu, M. Liserre, and A. V. Timbus, "Overview of control and grid synchronization for distributed power generation systems," IEEE Transactions on Industrial Electronics , vol. 53, no. 5, pp. 1398– 1409, Oct 2006.